ISSN 1070-4272, Russian Journal of Applied Chemistry, 2024, Vol. 97, No. 2, pp. 1–11. © Pleiades Publishing, Ltd., 2024.

CATALYSIS

Physicochemical Properties and NH_3-SCR Performance of Supported CeO_2–MnO_x Mixed Oxides Catalysts

Seyed Mahdi Mousavi[a,*], Parvaneh Nakhostin Panahi[b,*], and Aligholi Niaei[c,d]

[a] *Faculty of Chemistry, University of Kashan, Kashan, Iran*
[b] *Department of Chemistry, Faculty of Science, University of Zanjan, Zanjan, Iran*
[c] *Reactor & Catalyst Research Lab., Department of Chemical Engineering, University of Tabriz, Tabriz, Iran*
[d] *Department of physics, Faculty of Science, University of sakarya, Sakarya, Turkey*
**e-mail: mousavi.smahdi@kashanu.ac.ir*
***e-mail: panahi@znu.ac.ir*

Received November 24, 2023; revised March 12, 2024; accepted March 12, 2024

Abstract—CeO_2–MnO_x mixed oxides supported on different carriers (ZSM-5, TiO_2, and SAPO-34) were prepared by the sol-gel combustion method and evaluated for the selective catalytic reduction of NO with NH_3. The physicochemical properties of the samples were determined by using XRD, TEM, N_2 adsorption (BET method), H_2-TPR, and NH_3-TPD. The Ce–Mn/TiO_2 exhibited a higher NO conversion than Ce–Mn/ZSM-5 in the 100-200°C temperature range, but the NO conversion of Ce–Mn/ZSM-5 increases with reaction temperature (being the N_2 selectivity close to 100%) whereas, for Ce–Mn/TiO_2, the N_2 selectivity extremely decreases. The reducibility and surface acidity of samples seems to explain the catalytic performance. Thus, although the reducibility of Ce–Mn/ZSM-5 and Ce–Mn/TiO_2 was similar, the large number of surface acid sites of Ce–Mn/ZSM-5 could be a plausible reason for its excellent SCR activity. In fact, the superior SCR activity of Ce–Mn/ZSM-5 (94% NO conversion and 95% N_2 selectivity at 300°C) is related to the presence of well-dispersed Ce–Mn mixed oxide nanoparticles, high reducibility, and a large number of surface acid sites.

Keywords: cerium, mixed oxide, ZSM-5, TiO_2, SAPO-34, NH_3-SCR

DOI: 10.1134/S1070427224020034

INTRODUCTION

The dangerous effects of nitrogen oxides (NO_x) including the formation of photochemical smog and acid rain, the depletion of the stratospheric ozone layer as well as respiratory diseases are well documented [1]. In the last two decades, great efforts have been done by researchers to control the emission of NO_x from mobile and stationary sources [2–4]. The selective catalytic reduction (SCR) of NO_x with ammonia (NH_3-SCR) is a well-known low-cost and highly efficient technology for NO_x emissions reduction from stationary sources. For NH_3-SCR, ammonia is used as a reductant reacting with NO to convert this gas into N_2, N_2O, and H_2O via catalytic reactions [5–7].

Many catalytic systems including noble, transition, and rare earth metal-containing catalysts (unsupported, supported, and/or their mixed oxides) have been reported to be active for NH_3-SCR of NO_x [8–14]. Although most of the developed catalysts are highly active for the process, the current trend is to develop low-temperature catalysts more selective to N_2. Manganese oxides (MnO_x) are widely used as low-temperature NH_3–SCR catalysts because Mn presents different oxidation states, being able to easily close the catalytic cycle.[5] In recent years, ceria mixed oxide catalysts have been also investigated as SCR catalysts due to their high oxygen storage and release capacity as well as their redox properties [15–17]. Among them, CeO_2–MnO_x mixed oxides present an extraordinarily high performance in the low-temperature SCR of NO_x [18–20].

For industrial applications, the mixed oxide catalysts are usually supported by different carriers such as zeolites, activated carbons, TiO_2, and Al_2O_3 [20–22]. In this sense, it is well known that the supports play a significant role in the catalytic activity in SCR

reaction [9, 20, 23]. During the NH_3-SCR reaction on the supported catalyst, the reactants (NO_x, NH_3) and the catalyst are involved in the adsorption-desorption process and redox reactions [24, 25]. As a consequence, the catalyst behavior is related to: (*i*) the affinity towards NO_x and NH_3 and (*ii*) the redox properties. The adsorption-desorption process depends on the acid-base properties of the catalyst, which are mainly related to the acid-base support properties [21, 22, 26]. In other words, the efficiency of the catalytic systems in the SCR process is mostly based on the nature of active sites and the properties of the support [25].

Comparative studies of metal-based catalysts supported on different carriers (zeolites, TiO_2, Al_2O_3, SiO_2, activated carbons) have been reported for SCR of NO_x. Jin et al. [22]. compared the SCR behavior of two Ce–Mn oxide catalysts supported on TiO_2 and Al_2O_3. They found that the activities of these catalysts were relatively different, showing the Ce–Mn/TiO_2 better low-temperature SCR activity than Ce–Mn/Al_2O_3. Liu et al [25]. investigated the SCR performance of iron oxide catalysts supported on TiO_2, Al_2O_3, and beta-zeolite and found that the order of catalytic activity was Fe/zeolite >> Fe/TiO_2>> Fe/Al_2O_3.

Considering the above-described situation, a systematic study about the effect of support properties on the activity for NH_3–SCR of NO_x using supported CeO_2–MnO_x mixed oxide would be very useful in order to relate the catalyst properties with the catalyst's performance. Therefore, the aim of the present work is to analyze the effect of the support properties on the activity for NH_3–SCR of NO_x of a series of supported CeO_2–MnO_x mixed oxide catalysts. For that purpose, CeO_2–MnO_x mixed oxides supported on three different carriers (H-ZSM-5, SAPO-34, and TiO_2) -with high surface area, high mechanical strength, and high thermal stability as well as suitable acid-base properties - were prepared by sol-gel combustion method and characterized. The obtained results have been compared in terms of de-NO_x activity and selectivity to N_2, focusing attention on the effect of the physicochemical properties of the supports on the catalytic activity.

EXPERIMENTAL

Catalysts synthesis. Commercial supports were supplied by different manufacturers: H-ZSM-5 from ZEOCHEM® Int. (SiO_2/Al_2O_3: 50, Specific Surface Area (SSA): 376 m^2g^{-1}, Average Particle Size (APS): 100 nm), P25 TiO_2 from EVONIK (crystal structure: Anatas, SSA: 227 m^2g^{-1}, APS: 21 nm) and SAPO-34 from China Catalyst Chemistry (SSA: 600 m^2g^{-1}, APS: 37 nm). The sol-gel combustion method was employed for the synthesis and deposition of CeO_2–MnO_x mixed oxide on these supports. Our preliminary studies [18] showed that the CeO_2–MnO_x mixed oxide with Mn/(Ce+Mn) molar ratio of 0.25 (denoted as CeO_2–MnO_x (0.25)) showed the highest SCR activity. Therefore, in this study, supported CeO_2–MnO_x (0.25) mixed oxides with a 20 wt. % loading was prepared using the three carriers and the catalysts were denoted as 20 wt % Ce–Mn/support. For ZSM5, the effect of mixed oxide loading was analyzed and the catalysts were denoted as *X* wt % Ce–Mn/support (*X* = 10, 20, and 30).

In the sol-gel combustion method used for the synthesis of catalysts, the stoichiometric amount of cerium (III) nitrate hexahydrate (Merck) and manganese (II) nitrate tetrahydrate (Merck) were dissolved in distilled water according to the desired molar ratio (0.25). The total concentration of metallic ions was kept at 0.1 M. After, 1 g of the support was added to the solution and vigorously stirred at 60°C for 30 min. Then the citric acid, as the complexation agent, was added to the suspension (the molar ratio citric acid /total metallic ions was 1). The above mixture was evaporated by continuous stirring at 60°C for several hours. Subsequently, the resulting materials were dried at 100°C overnight followed by heating in air at 300°C for 1 h to decompose the organic species. Finally, the obtained materials were calcined in air at 550°C for 4 h.

Catalysts characterization. The phase composition of the catalysts was determined by X-ray powder diffraction (XRD) using a Siemens D5000 dual goniometer diffractometer by a graphite monochromator CuK_α radiation (λ = 1.54 nm).

Transmission Electron Microscopy (TEM) studies were performed using a JOEL (JEM-2010) microscope. For TEM analysis, a few droplets of an ultrasonically dispersed suspension of each sample in ethanol were placed on a copper grid with lacey carbon film and dried at ambient conditions.

The specific surface areas of the catalysts and supports were calculated by N_2 adsorption (at 77) data using the BET method (Micrometrics ASAP 2010).

Before adsorption, the samples were outgassed at 453 for 4 h.

The reducibility of supported catalysts was determined by Temperature Programmed Reduction with H_2 (H_2-TPR) experiments in a Micrometritics 2910 apparatus. Before the H_2-TPR analysis, the samples were pretreated by heating in air flow at 500°C for 30 min and cooling down to 50°C in 20% O_2/He. The hydrogen consumption was determined using a gaseous mixture composed of 3 vol % H_2 in Ar (flow rate 15 cm^3 min^{-1}) and a linear heating rate of 10°C min^{-1} from the 50–900°C temperature range.

Temperature Programmed Desorption of NH_3 (NH_3-TPD) was carried out to determine the acidity of the catalysts. Before the NH_3-TPD experiments, the samples were pre-treated by heating in air at 500°C for 30 min (to stabilize and remove of any possible adsorbed gases on the samples) and then cooled to 100°C under 20 % O_2 in He. Ammonia adsorption was carried out using a 5% NH_3/He gas mixture (flow rate 40 cm^3 min^{-1}) for 30 min at 100°C. Physically adsorbed ammonia was removed by purging with helium (flow rate 25 cm^3 min^{-1}) at 100°C for 30 min. Finally, NH_3-TPD was performed by linearly increasing the temperature (10°C min^{-1}) from 100 to 550°C.

Catalytic activity tests. The SCR activity of prepared catalysts was evaluated in a fixed bed quartz reactor (i.d. = 10 mm) at atmospheric pressure. In all the tests, 0.2 g catalyst was placed between quartz wool plugs, and the feed gas mixture containing 1000 ppm NO, 1000 ppm NH_3, 5% O_2, and Ar as balance was fed into the reactor at a total flow rate of 200 cm^3 min^{-1}, which corresponded to a gas hourly space velocity (GHSV) of 12000 h^{-1}. The SCR experiments were carried out at a temperature range of 100-400°C with a step of 50°C. The concentration of NO and NO_2 at the inlet and outlet of the reactor was monitored by a Flue Gas Analyzer (Testo 350M/XL). A gas Chromatograph (SHIMADZU model 2010 plus) equipped with a Thermal Conductivity Detector (TCD) and a molecular sieve column (HP-Molesieve, 0.53 mm diameter, 30 m length) was used to determine the concentration of N_2O and N_2. According to the concentration of NO, NO_2, N_2O, and N_2 in the inlet and outlet flow, the NO conversion (%) and the N_2 (%) selectivity were calculated using the following equations:

$$\text{NO Conversion} = \frac{([\text{NO}])_{\text{in}} - ([\text{NO}])_{\text{out}}}{([\text{NO}])_{\text{in}}} \times 100, \quad (1)$$

$$\text{N}_2\ \text{Selectivity} = \frac{([\text{N}_2])_{\text{out}}}{([\text{N}_2] + [\text{N}_2\text{O}])_{\text{out}}} \times 100. \quad (2)$$

The subscripts in and out indicate the inlet and outlet concentration at steady state, respectively.

RESULTS AND DISCUSSION

Characterization of Supported Mixed Oxide Catalysts

BET, XRD, and TEM analysis. The structural and physicochemical properties of supported Ce–Mn mixed oxides were determined by BET, XRD, and TEM analysis. The BET surface area of the supports has been also included as a reference. The BET surface areas of supported CeO_2–MnO_x catalysts are compared in Table 1 (The N_2 adsorption/desorption isotherms are presented in appendix 1). The 20 wt % Ce–Mn/SAPO-34 catalyst presents the largest specific surface area, whereas the 20 wt % Ce–Mn/TiO_2 features the lowest one. It is observed that the surface area of all the supports decreases after the formation of CeO_2–MnO_x on the catalyst surface, due to the partial blockage of the pores by CeO_2–MnO_x particles [20, 27]. Note that for TiO_2 and SAPO-34 supports the BET surface area noticeably decreases and, that for ZSM-5 support, the surface area decreases as the CeO_2–MnO_x content increases as a consequence of the partial blockage of ZSM-5 pores due to the growing of CeO_2–MnO_x crystallites.

Table 1. BET surface area of the carriers and supported CeO_2–MnO_x

Samples	BET surface area, m^2/g
TiO_2	227
ZSM-5	376
SAPO-34	600
10 wt % Ce–Mn/ZSM-5	369
20 wt % Ce–Mn/ZSM-5	340
30 wt % Ce–Mn/ZSM-5	238
20 wt % Ce–Mn/TiO_2	55
20 wt % Ce–Mn/SAPO-34	361

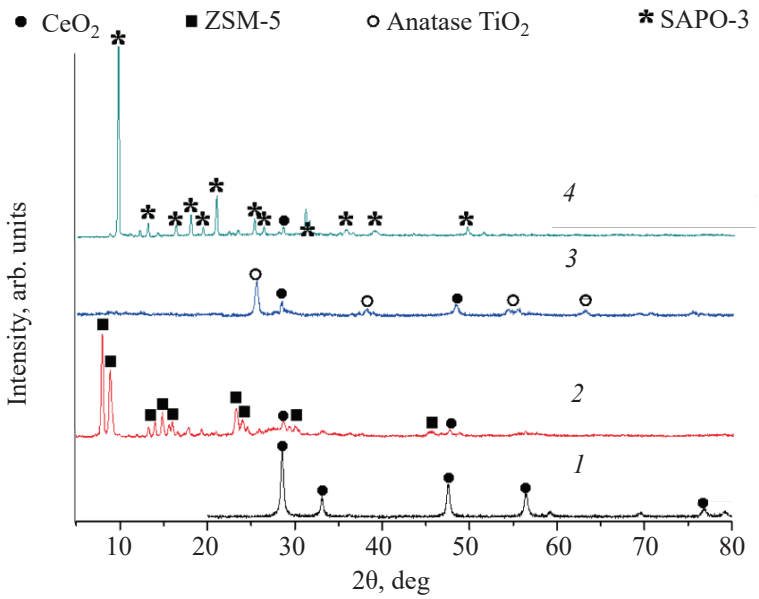

Fig. 1. Powder X-ray diffraction patterns of: (*1*) CeO_2–MnO_x (0.25), (*2*) 20 wt % Ce–Mn/ZSM-5, (*3*) 20 wt % Ce–Mn/TiO_2 and (*4*) 20 wt % Ce–Mn/SAPO-34.

The XRD patterns of the CeO_2–MnO_x (0.25) and Ce–Mn supported on ZSM-5, TiO_2, and SAPO-34 are shown in Fig. 1. The pattern of CeO_2–MnO_x (0.25) shows the diffraction peaks (at 2θ = 28.55°, 33.09°, 47.50°, 56.37°, 59.11°, 69.44°, 76.73°, and 79.11°) corresponding to ceria with a cubic fluorite structure (JCPDS No. 34-0394). No diffraction peak related to Mn phase was detected, which is in agreement with that reported in the literature [18, 28] and indicates that Mn ions seem to be incorporated into the Ce lattice during sol-gel combustion process to form a solid solution, or that Mn phases present a crystallite size under the detection limit of the XRD technique.

All the characteristic peaks corresponding to H-ZSM-5 (JCPDS files: PDF#42-0023), anatase TiO_2 (JCPDS files: PDF#21-1272), and SAPO-34 with chabazite phase (JCPDS files: PDF#47-0429) are identified in the patterns of supported CeO_2–MnO_x (0.25).

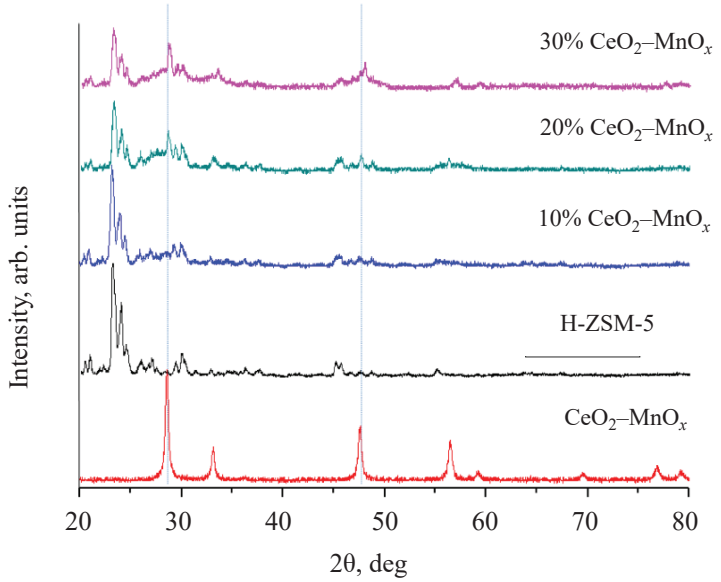

Fig. 2. Powder X-ray diffraction patterns of CeO_2–MnO_x supported on ZSM-5 with different loading: (*1*).

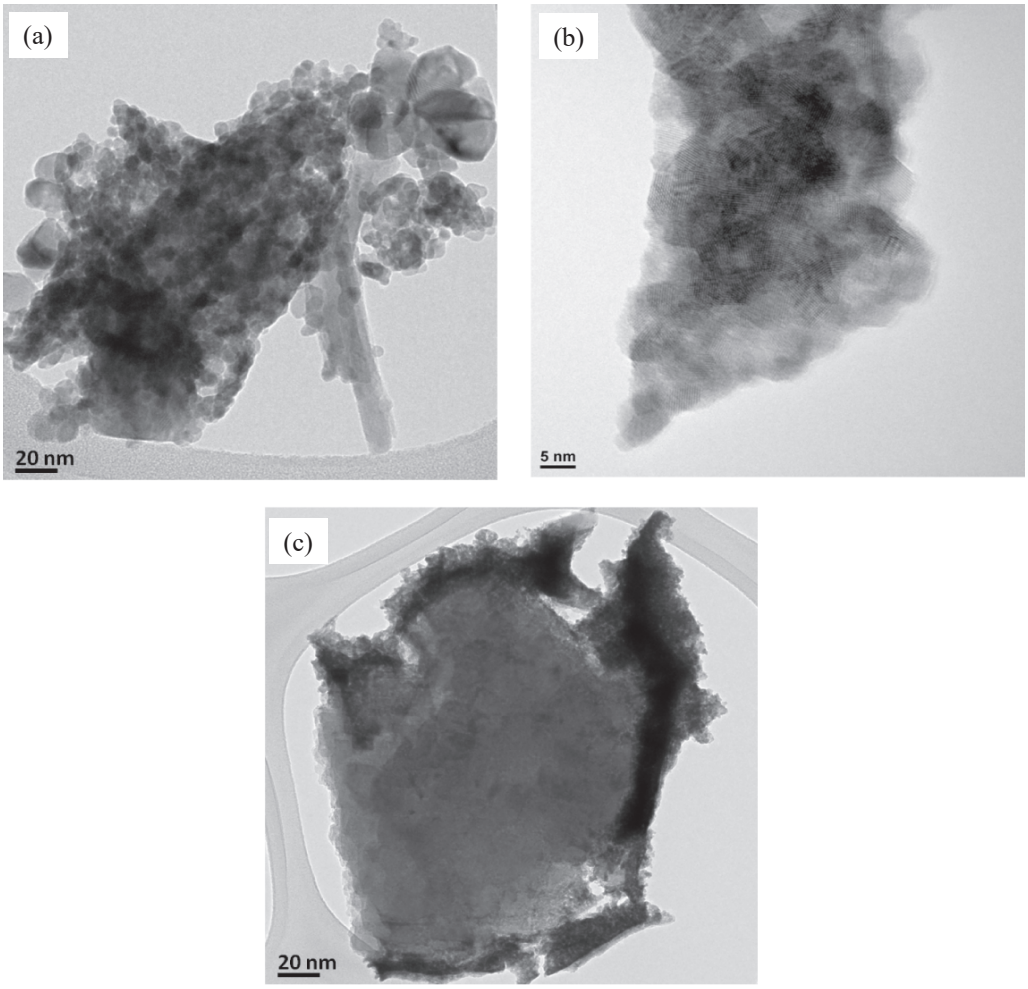

Fig. 3. TEM images of Ce–Mn/ZSM-5: (a, b) 20 wt %, (c) 30 wt %.

It suggests that the original structure of the supports was not destroyed during the sol-gel combustion synthesis of mixed oxide. Indeed, in these supported samples, the diffraction peaks corresponding to the ceria phase (cubic fluorite) present a weak intensity and there is no observed diffraction peak corresponding to Mn phase.

The XRD patterns of Ce–Mn/ZSM-5 with different loadings are compared in Fig. 2. In the XRD pattern of 10 wt % Ce–Mn/ZSM-5, the characteristic peaks due to the phases containing Ce or Mn are not observed, implying that nanosized metal oxides were highly dispersed on the support [13, 27]. However, in the sample 20 wt % Ce–Mn/ZSM-5, weak peaks due to the Ce–Mn phases appear, indicating that Ce–Mn mixed oxide is formed on the surface of the zeolite. The intensity of the peaks corresponding to Ce–Mn mixed oxide in 30 wt % Ce–Mn/ZSM-5 is clearly larger due to the agglomeration of mixed oxide particles on the zeolite surface [27]. It can be also observed that as the Ce–Mn content increases, the intensity of diffraction peaks of ZSM-5 decreases, suggesting the introduction of the metal oxide particles into the ZSM-5 channels and, also, the decrease of the crystallinity samples degree.

In order to examine the morphology and dispersion of active sites in the Ce–Mn/ZSM-5 with different loading, TEM images have been obtained and they are shown in Figs. 3a–3c. The bright-colored area represents ZSM-5 and the dark area corresponds to the Ce–Mn particles. In Fig. 3b it is possible to observe the characteristic channels of the ZSM-5 zeolite, and this confirms that the structure of the ZSM-5 didn't change after the incorporation of the Ce–Mn mixed oxide on the surface. The TEM images of the 20 wt % Ce–Mn/ZSM-5 and 30 wt % Ce–Mn/ZSM-5 catalysts (Figs. 3a,

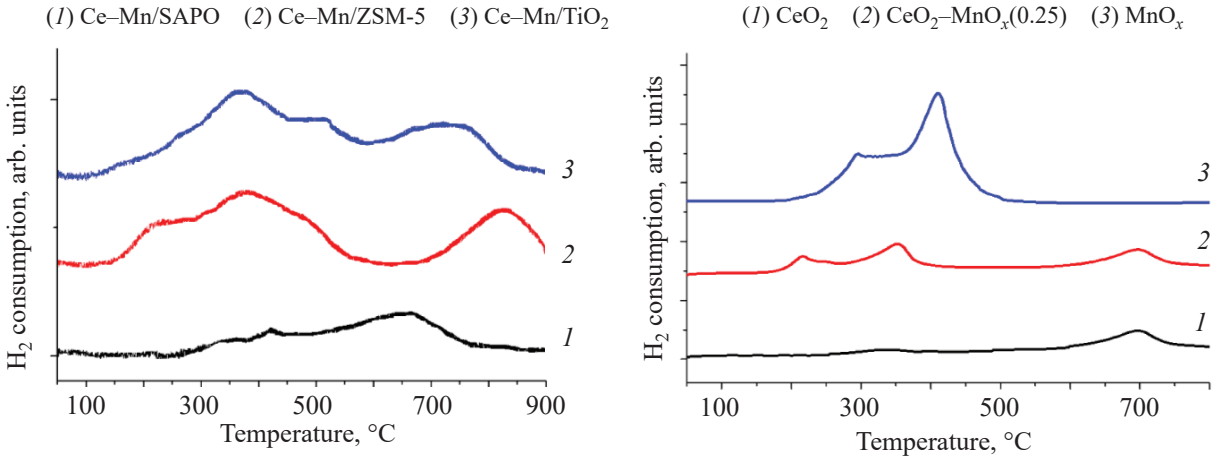

Fig. 4. H_2-TPR profile of: (a) supported CeO_2–MnO_x, (b) pure CeO_2, MnO_x and CeO_2–MnO_x mixed oxide.

3c) display that the distribution of the particles of Ce–Mn mixed oxide depends on the CeO_2–MnO_x loading and that a high dispersion of CeO_2–MnO_x particles was attained for the 20 wt % loading, which agrees with the results obtained by XRD. Thus, for the 20 wt % Ce–Mn/ZSM-5 (Fig. 3a) the particles of Ce–Mn mixed oxides are well dispersed on the zeolite's channels, whereas for the 30 wt % Ce–Mn/ZSM-5 catalyst (Fig. 3c) the CeO_2–MnO_x particles are localized on the external channels of ZSM-5.

TPR and NH_3-TPD analysis. The NH_3–SCR of NO_x over metal oxide catalysts is a redox process, therefore the reducibility of the metal oxide is known to be one of the properties determining the catalytic performance for SCR of NO_x [29, 30]. Thus, the enhancement of the catalyst's reducibility should improve the NO_x oxidation to nitrites and/or nitrates and also NH_3 activation to NH_2OH and thereby, increases the efficiency of NO_x reduction by ammonia [13,18]. The reducibility of the supported CeO_2–MnO_x mixed oxide catalysts was explored by using H_2-TPR analysis and the corresponding H_2-TPR profiles are shown in Fig. 4a, meanwhile, for comparative purpose, the reduction profile of pure CeO_2, MnO_x and unsupported CeO_2–MnO_x are featured in Fig. 4b. According to this figure, the pure CeO_2 shows two low-intensity reduction peaks located at around 350 and 720°C, which correspond to the reduction of surface and bulk Ce^{4+} to Ce^{3+} respectively [15, 18]. The H_2-TPR profile of pure MnO_x displays two overlapped reduction peaks with maximums at 300 and 420°C. The MnO is the final reduction state of various Mn species. Therefore, the low-temperature peak is due to the reduction of MnO_2 to Mn_2O_3 and the reduction of Mn_2O_3 to MnO is suggested as the reduction process for the high-temperature signal [19].

The H_2-TPR profile of CeO_2–MnO_x mixed oxide shows three broad reduction peaks around 220, 350, and 710°C (Fig. 4b). Compared with the H_2-TPR profiles of pure CeO_2 and MnO_x, it is obvious that the first peak can be attributed to the stepwise reduction of Mn^{+4} ions which embedded into the ceria lattice (Mn^{+4}–O–Ce^{+4}) and the second peak can be assigned to the combined reduction of Mn^{3+} to Mn^{2+} and surface Ce^{4+}ions. The weak peaks around 710°C could be due to the reduction of ceria bulk. It is noteworthy that for CeO_2–MnO_x mixed oxide, the reduction peaks of Mn shift to lower temperatures, which suggests that there is a synergistic effect between the Mn and Ce species [18, 29].

In Fig. 4a, it is observed that 20 wt % Ce–Mn/SAPO-34 exhibits a very broad reduction peak with maxima at 320, 430, and 690°C. Compared with the TPR profiles of pure CeO_2 and MnO_x, the first and second maxima can be attributed to the stepwise reduction of highly dispersed MnOx phases and, the third TPR maximum corresponds to the reduction of ceria bulk. According to the H_2-TPR profile of 20 wt % Ce–Mn/SAPO-34, it seems that the reduction peaks of Mn did not shift to lower temperatures. Consequently, it seems that mixed oxide is not formed on the surface of SAPO-34 and that, instead, well-dispersed nanosized MnO_x (not observed in XRD patterns due to its small size) and CeO_2 phases may be formed on the surface of SAPO-34.

The H_2–TPR profile of 20 wt % Ce–Mn/ZSM-5 (Fig. 4a) shows two peaks centered at 220 and 360°C, which corresponds to the reduction of Mn^{+4} ions located

in the ceria lattice (Mn^{+4}–O–Ce^{+4}) and to the reduction of surface Ce^{+4} ions. In addition, there is a broad peak with a maximum at 800°C that can be attributed to the reduction of bulk Ce^{+4} ions. This result is consistent with that reported for the CeO_2–MnO_x mixed oxide (Fig.4b) and reveals that the Ce–Mn mixed oxide is formed on the surface of ZSM-5.

Finally, the H_2-TPR profile of 20 wt % Ce–Mn/TiO_2 is qualitatively similar to 20 wt % Ce–Mn/ZSM-5 and shows peaks at 220, 360, and 750°C, but in addition, a peak at 450 ºC with a relatively lower intensity appears. Thus, CeO_2–MnO_x mixed oxide is formed on the surface of TiO_2 support but the peak at 450°C suggests that a fraction of Mn is not incorporated into the CeO_2–MnO_x mixed oxide structure but it appears on the TiO_2 surface like a MnO_x oxide. Thus, the H_2-TPR results reveal that CeO_2–MnO_x mixed oxides are formed on ZSM-5 and TiO_2 supports whereas nanosized MnO_x and CeO_2 phases are formed on SAPO-34. Regarding the synergistic effect between the Mn and Ce species in CeO_2–MnO_x mixed oxide, the order of reducibility of prepared catalysts is 20 wt % Ce–Mn/ZSM-5 >= 20 wt % Ce–Mn/TiO_2> 20 wt % Ce–Mn/SAPO-34.

Figure 5 shows the normalized NH_3-TPD profiles for CeO_2–MnO_x mixed oxides supported on SAPO-34, ZSM-5, and TiO_2. The acid surface properties of the catalysts play an important role in the adsorption-desorption of the reactants in the NH_3-SCR reaction [31-33]. The relative position of the NH_3 desorption peaks in NH_3-TPD profiles gives information about the strength of the catalyst's acid sites. The NH_3-TPD profile of 20 wt % Ce–Mn/SAPO-34 presents, also, two desorption peaks. The low-temperature peak around 180°C, is assigned to the desorption of NH_3 adsorbed on the weak Brønsted acid sites as surface hydroxyls, whereas the broad high-temperature peak in the temperature range of 250–500°C could be attributed to the desorption of the NH_3 adsorbed on the structural Brønsted acid sites that are referred as moderate and strong acidity sites [30, 31].

The NH_3-TPD profile of 20 wt % Ce–Mn/ZSM-5 shows two low-intensity desorption peaks: i) the low-temperature desorption peak around 200°C is assigned to weakly adsorbed NH_3 and ii) the weak broad peak around 400°C is assigned to strongly adsorbed NH_3 arising from NH_3 bounded to the protons of the zeolite. The normalized NH_3-TPD profile of 20 wt % Ce–Mn/TiO_2 (Fig. 5) shows a very broad and very low-intensity peak from 130-400°C, which could be attributed to the desorption of the NH_3 physisorbed on the weak acid sites and likely connected to Brønsted acid sites. The peak related to NH_3 desorbed from Lewis's acid sites of the TiO_2 appears at 570–680°C (not shown) [22].

(*1*) 20 wt % Ce–Mn/SAPO-34 (*2*) 20 wt % Ce–Mn/ZSM-5 (*3*) 20 wt % Ce–Mn/TiO_2

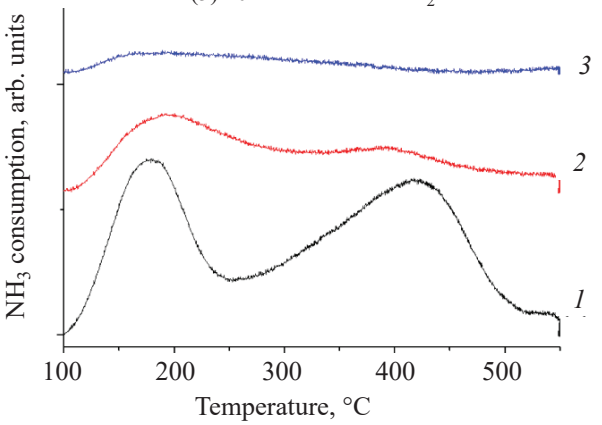

Fig. 5. NH_3-TPD of 20 wt % CeO_2–MnO_x supported on different carriers.

Table 2 shows the amount of the desorbed ammonia calculated from the NH_3-TPD results. Based on the NH_3-TPD results (Fig. 5 and Table 2), it is clear that the 20 wt % Ce–Mn/SAPO-34 catalysts present the highest NH_3 adsorption capacity and, consequently, have the largest number of surface acid sites and, that 20 wt % Ce–Mn/TiO_2 presents a very low capacity for NH_3 adsorption.

Activity of Supported Mixed Oxide Catalysts

The NH_3-SCR performance of the CeO_2–MnO_x catalysts supported on different carriers (20 wt % loading) in terms of NO conversion and N_2 selectivity as a function of the reaction temperature is shown in Fig. 6. The NH_3-SCR performance of unsupported

Table 2. NH_3 uptake calculated from the NH_3-TPD data of supported CeO_2–MnO_x catalysts

Catalyst	20 wt % Ce–Mn/SAPO-34	20 wt % Ce–Mn/ZSM-5	20 wt % Ce–Mn/TiO_2
Total NH_3 uptake, μmole/g	1482	465	56

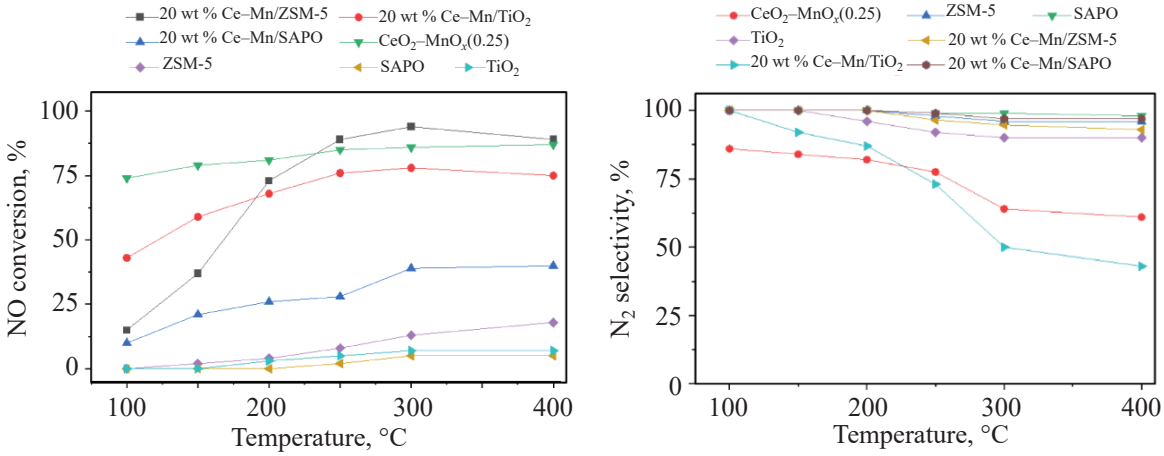

Fig. 6. NH_3-SCR performance of 20 wt % CeO_2–MnO_x on different supports: (a) NO conversion, (b) N_2 selectivity.

CeO_2–MnO_x, ZSM-5, SAPO-34 and TiO_2 are also presented in Fig. 6 as reference. As shown in Fig. 6a, the unmodified supports exhibited quite low activity at all temperatures. The Ce–Mn/SAPO-34 had low activity at the different temperatures tested. In the low-temperature range (100–200°C), the Ce–Mn/TiO_2 exhibited a higher NO conversion than Ce–Mn/ZSM-5 but, at reaction temperatures higher than 200°C, the NO conversion of Ce–Mn/ZSM-5 becomes to be higher than that of the Ce–Mn/TiO_2. It is noteworthy that as the reaction temperature increases, the N_2 selectivity of Ce–Mn/TiO_2 extremely decreases, whereas the Ce–Mn/ZSM-5 catalyst is kept close to 100% in the 100-400°C temperature range. Thus, it can be concluded that Ce–Mn/ZSM-5 exhibits better NH_3-SCR performance than Ce–Mn/TiO_2: a NO conversion of 89% at 250°C and 94% at 300°C, being the N_2 selectivity close to 100% on the whole temperature range used. However, the NO conversion of the Ce–Mn/ZSM-5 decreases above 300°C, probably due to the preferential oxidation of NH_3 by oxygen.

Considering the BET surface area data (Table 1), it seems that there is no relationship between the SCR performance of supported CeO_2–MnO_x and the BET surface area. Taking into account the H_2–TPR results (Fig. 4), it seems that, the high NO reduction activity of 20 wt % Ce–Mn/ZSM-5 and 20 wt % Ce–Mn/TiO_2 catalysts are related to the presence of easily reducible CeO_2–MnO_x mixed oxide on these two supported catalysts. Although the reducibility of 20 wt % Ce–Mn/ZSM-5 and 20 wt % Ce–Mn/TiO_2 was similar (H_2-TPR results in Fig. 4), the larger amount of surface acid sites of the 20 wt % Ce–Mn/ZSM-5 respect to 20 wt % Ce–Mn/TiO_2 (Table 2) could explain its higher SCR activity. Based on the large number of acid sites of 20 wt % Ce–Mn/SAPO-34 (Fig 5 and Table 2), a high SCR activity could be expected. However, the low reducibility of 20 wt % Ce–Mn/SAPO-34 (Fig. 5) overcomes the strong acidity, resulting in a low SCR performance.

As shown in Fig. 6a, the unsupported CeO_2–MnO_x mixed oxide presents a higher low-temperature NO conversion than CeO_2–MnO_x supported on ZSM-5, while as the temperature increases, the NO conversion over 20 wt % Ce–Mn/ZSM-5 also increases, However, in terms of the N_2 selectivity, the unsupported CeO_2–MnO_x catalyst presents much lower N_2 selectivity than 20 wt % Ce–Mn/ZSM-5 catalyst in the whole range of temperature analyzed. It is noteworthy that, the combination of cerium, manganese, and zeolite, as catalyst support, modifies the acid and the redox properties which are significant factors for the NH_3–SCR process.

According to the above results and interpretations, a proposed NH_3-SCR reaction mechanism on the CeO_2–MnO_x/ZSM-5 was illustrated in Fig. 7. Due to the presence of different oxidation states of Ce and Mn cations in the CeO_2–MnO_x lattice, there are a large amount of oxygen vacancies. By adsorbing the O_2 on the surface of the catalysts, a numerous surface activated oxygen is produced (as shown in Fig. 8). NO could be easily adsorbed and activated on the catalytic sites and then could react with surface activated oxygen to produce NO_2. Meanwhile, the adsorption and activation of NH_3 on acidic sites could be done and generated

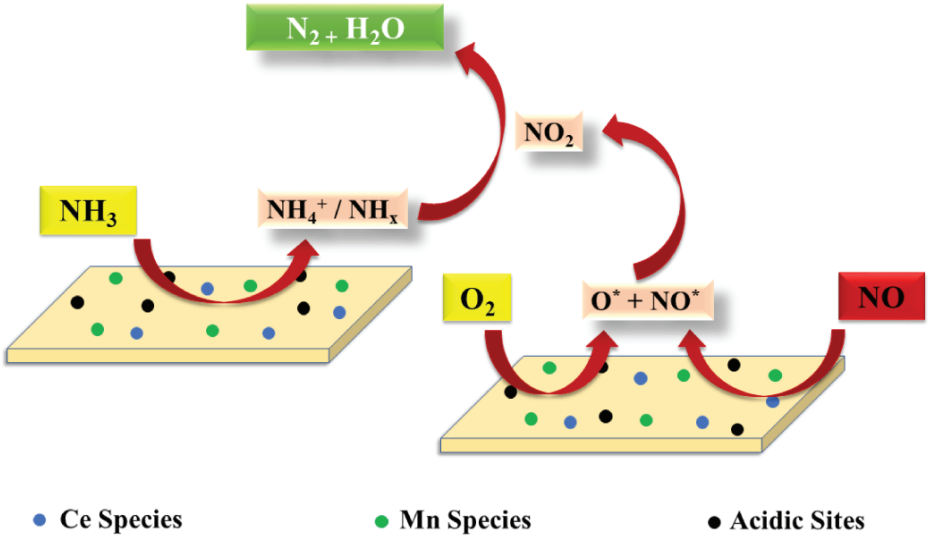

Fig. 7. Proposed NH_3-SCR reaction mechanism on the CeO_2–MnO_x/ZSM-5.

NH_4^+ and NH_x amines. Finally, the produced NH_4^+ and NH/NH_2 could react with NO_2 on the active sites and generate N_2.

Figure 8 shows the catalytic performance of CeO_2–MnO_x mixed oxide supported on ZSM-5 with different loadings (between 10–30 wt %). It can be observed that the catalytic performance of CeO_2–MnO_x supported on ZSM-5 catalysts is a function of the CeO_2–MnO_x loading: as the of CeO_2–MnO_x content increases, the NO conversion also increases due to the presence of a larger number of active sites. However, the observed improvement of the catalytic performance achieves a limit when the loading is higher than 20 wt % and the NO conversion decreases for 30 wt % loading. According to TEM results (Fig. 3), this fact seems to be due to a metal particle agglomeration leading to the formation of larger metal crystallites blocking the pores and the active sites of the zeolite [12].

CONCLUSIONS

From the analysis of the physicochemical properties of CeO_2–MnO_x mixed oxides supported on different carriers (ZSM-5, TiO_2, and SAPO-34) and their NH_3-SCR performance, the following conclusion can be drawn:

The XRD and TEM results proved that the original structure of supports is not destroyed during the preparation of mixed oxide by sol-gel combustion method.

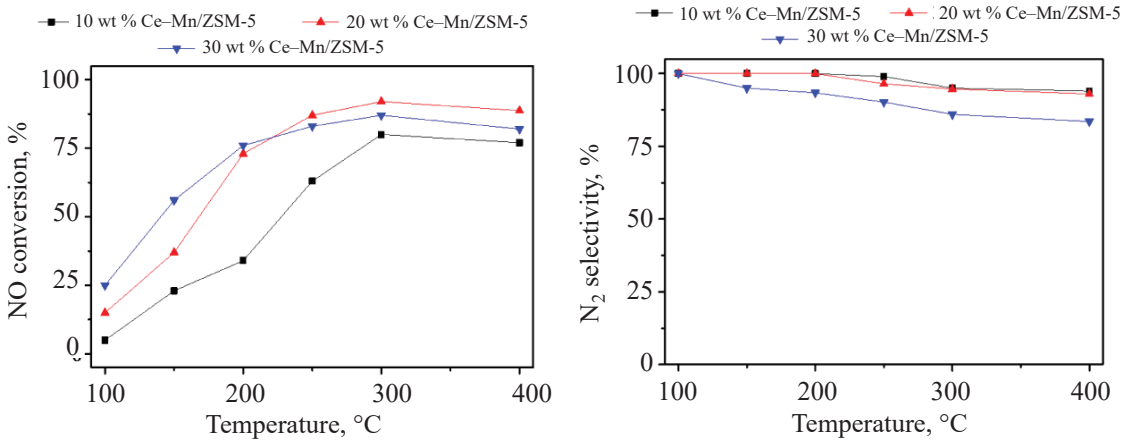

Fig. 8. NH_3-SCR performance of CeO_2–MnO_x supported on ZSM-5 with different loading: (a) NO conversion, (b) N_2 selectivity.

The catalytic performance for the NH_3-SCR depends on the support. The 20 wt % Ce–Mn/ZSM-5 presents the best NH_3–SCR performance: a NO conversion of 89% at 250°C and 94% at 300°C, with an N_2 selectivity close to 100% on the whole temperature range tested. The high reducibility and surface acidity, as well as the presence of well-dispersed Ce–Mn mixed oxide nanoparticles, seem to justify the superior SCR performance of 20 wt % Ce–Mn/ZSM-5 catalyst.

The BET data indicated that there is no direct relationship between the SCR performance of supported CeO_2–MnO_x and the BET surface area.

For ZSM5-based catalysts, the catalytic performance also depends on the amount of mixed oxide and, under the specific conditions used, the 20 wt % Ce–Mn/ZSM-5 presents the largest NO conversion (94%) and N_2 selectivity (95%) at 300°C. The obtained results are very close to the results reported in Ran et. al [33], of course, at a slightly higher temperature.

SUPPLEMENTARY INFORMATION

The online version contains supplementary material vailable at https://doi.org/10.1134/S1070427224020034.

ACKNOWLEDGMENTS

The authors would like to gratefully acknowledge the University of Tabriz, Zanjan, and Kashan for financial and other support.

FUNDING

This work was supported by ongoing institutional funding. No additional grants to carry out or direct this particular research were obtained.

CONFLICTS OF INTEREST

There are no conflicts of interest to declare.

REFERENCES

1. Roy, S., Hegde, M and Madras., G., *Appl. Energy.,* 2009, vol. 86, pp. 2283–2297.
2. Basfar, A.A., Fageeha, O.I., Kunnummal, N., Al-Ghamdi, S., Chmielewski, A.G., Licki, J., Pawelec, A., Tymiński, B., and Zimek, Z., *Fuel,* 2008, vol. 87, pp. 1446–1452.
3. Forzatti, P., *Appl. Catal. A: Gen.,* 2001, vol. 222, pp. 221–236.
4. Tang, X., Hao, J., Yi, H., and Li, J., *Catal. Today.,* 2007, vol. 126, pp. 406–411.
5. Kang, M., Park, E.D., Kim, J.M., and Yie, J.E., *Appl. Catal. A: Gen.,* 2007, vol. 327, pp. 261–269
6. Song, Z., Zhang, Q., Ning, P., Fan, J., Duan, Y., Liu, X., and Huang, Z., *J. Taiwan. Inst. Chem. Eng.,* 2016, vol. 65, pp. 149–161.
7. Holma, T., Palmqvist, A., Skoglundh, M., and Jobson, E., *Appl. Catal. B: Environ*., 2004, vol. 48, pp. 95–100.
8. Itoh, M., Iwamoto, J., Tajima, N., and Machida, K-I., *Chem. Phys.,* 2010, vol. 124, pp. 587–591.
9. Mousavi, S.M. and Nakhostin Panahi, P., *J. Taiwan. Inst. Chem. Eng.,* 2016, vol. 69, pp. 68–77.
10. Lin, F., Wu, X., and Weng, D., *Catal. Today.,* 2011, vol. 175, pp. 124–132.
11. Chen, Q-l., Guo, R-t., Wang, Q-s., Pan, W-g., Yang, N-z., Lu, C-z. and Wang, S-x., *J. Taiwan. Inst. Chem. Eng.,* 2016, vol. 64, pp. 116–123.
12. Mousavi, S.M., Niaei, A., Salari, D., Nakhostin Panah, P., and Samandari, M., *Environ. Technol.,* 2013, vol. 34, pp. 1377–1384.
13. Nakhostin Panahi, P., Salari, D., Niaei, A., and Mousavi, S., *J. Ind. Eng. Chem.,* 2013, vol. 19, pp. 1793–1799.
14. Amanpour, J., Salari, D., Niaei, A., Mousavi, S.M., and Nakhostin Panahi, P., *J. Environ. Sci. Health A.,* 2013, vol. 48, pp. 879–883.
15. Kongzhai, L., Hua, W., Yonggang, W., and Mingchun, L., *J. Rare Earths*., 2008, vol. 26, pp. 245–249.
16. Zahir, M.H., Suzuki, T., Fujishiro, Y., and Awano, M., *Mater. Chem. Phys.,* 2009, vol. 116, pp. 273–278.
17. Qi, G., *Appl. Catal. B, Environ.,* 2004, vol. 51, pp. 93–100.
18. Mousavi, S.M., Niaei, A., Gómez, M.J.I., Salari, D., Nakhostin Panahi, P., and Abaladejo-Fuentes, V., *Mater. Chem. Phys.,* 2014, vol. 143, pp. 921–928.
19. Mousavi, S.M., Salari, D., Niaei, A., Nakhostin Panahi, P., and Shafiei, S., *Environ. Technol.,* 2014, vol. 35, pp. 581–589.
20. Carja, G., Kameshima, Y., Okada, K., and Madhusoodana, C.D., *Appl. Catal. B: Environ.,*

2007, vol. 73, pp. 60–64.

21. Gao, X., Liu, S., Zhang, Y., Du, X., Luo, Z., and Cen, K., *Catal. Today.,* 2011, vol. 175, pp. 164–170.
22. Jin, R., Liu, Y., Wu, Z., Wang, H., and Gu, T., *Chemosphere.,* 2010, vol. 78, pp. 1160–1166.
23. Xu, W., Yu, Y., Zhang, C., and He, H., *Catal. Commun.,* 2008, vol. 9, pp. 1453–1457.
24. Illán-Gómez, M., Raymundo-Pinero, E., Garcıa-Garcıa, A., Linares-Solano, A., and de Lecea, C.S.-M., *Appl. Catal. B: Environ.,* 1999, vol. 20, pp. 267–275.
25. Liu, Z., Millington, P.J., Bailie, J.E., Rajaram, R.R., and Anderson, J.A., *Microporous Mesoporous Mater.,* 2007, vol. 104, pp. 159–170.
26. Sultana, A., Nanba, T., Haneda, M., and Hamada, H., *Catal. Commun.,* 2009, vol. 10, pp. 1859–1863.
27. Jodaei, A., Salari, D., Niaei, A., Khatamian, M., and Caylak, N., *Environ. Technol.,* 2011, vol. 32, pp. 395–406.
28. Mai, H., Zhang, D., Shi, L., Yan, T., and Li, H., *Appl. Surf. Sci.,* 2011, vol. 257, pp. 7551–7559.
29. Kang, M., Park, E.D., Kim, J.M., and Yie, J.E., *Catal. Today.,* 2006, vol. 111, pp. 236–241.
30. Snytnikov, P., Popova, M., Men, Y., Rebrov, E., Kolb, G., Hessel, V., Schouten, J and Sobyanin, V., *Appl. Catal. A: Gen.,* 2008, vol. 350, pp. 53–62.
31. Izadbakhsh, A., Farhadi, F., Khorasheh, F., Sahebdelfar, S., Asadi, M., and Feng, Y.Z., *Appl. Catal. A: Gen.,* 2009, vol. 364, pp. 48–56.
32. Ni, K., Peng, Y., Dai, G., Zhao, H., Huang, Z., Wu, X., Jing, G., Feng, W., and Yuan, Y., *J. Taiwan Inst. Chem. Eng.,* 2022, vol. 140, p. 104555.
33. Shi, Z., Peng, Q., Jiaqiang, E., Xie B., Wei, J., Yin, R., and Fu, G., *Fuel,* 2023, vol. 331, p. 125885.
34. Yan, R., Lin, S., Li, Y., Liu, W., Mi, Y., Tang, C., Wang, L., Wu, P., Peng, H., *J. Hazar. Mat.,* 2020, vol. 396, p. 122592.

Publisher's Note. Pleiades Publishing remains neutral with regard to jurisdictional claims in published maps and institutional affiliations.